CrossMark

J̶M RAPIDS

On the criteria of large cavitation bubbles in a tube during a transient process

Peng Xu[1,2], Shuhong Liu[1], Zhigang Zuo[1],† and Zhao Pan[2],†

[1]Department of Energy and Power Engineering, and State Key Laboratory of Hydro Science and Engineering, Tsinghua University, Beijing 100084, PR China

[2]Department of Mechanical and Mechatronics Engineering, University of Waterloo, University of Waterloo, 200 University Avenue West, Waterloo, Ontario N2L 3G1, Canada

Extreme cavitation scenarios, such as water column separations in hydraulic systems during transient processes caused by large cavitation bubbles, can lead to catastrophic destruction. In the present paper, we study the onset criteria and dynamics of large cavitation bubbles in a tube. A new cavitation number $Ca_2 = l^{*-1} Ca_0$ is proposed to describe the maximum length L_{max} of the cavitation bubble, where l^* is a non-dimensional length of the water column indicating its slenderness, and Ca_0 is the classic cavitation number. Combined with the onset criteria for acceleration-induced cavitation ($Ca_1 < 1$, Pan *et al.*, *Proc. Natl Acad. Sci. USA*, vol. 114, 2017, pp. 8470–8474), we show that the occurrence of large cylindrical cavitation bubbles requires both $Ca_2 < 1$ and $Ca_1 < 1$ simultaneously. We also establish a Rayleigh-type model for the dynamics of large cavitation bubbles in a tube. The bubbles collapse at a finite end speed, and the time from the maximum bubble size to collapse is $T_c = \sqrt{2}\sqrt{lL_{max}}\sqrt{\rho/p_\infty}$, where l is the length of the water column, L_{max} is the maximum bubble length, ρ is the liquid density and p_∞ is the reference pressure in the far field. The analytical results are validated against systematic experiments using a modified 'tube-arrest' apparatus, which can decouple acceleration and velocity. The results in the current work can guide design and operation of hydraulic systems encountering transient processes.

Key words: cavitation, bubble dynamics

1. Introduction

Cavitation involves explosive growth of vapour bubbles subjected to a quick local pressure reduction, and subsequent destructive collapses. Examples of cavitation effects include sharp head drop of hydraulic machinery, erosion of spillways and ultrasonic cleaning

† Email addresses for correspondence: zhigang200@tsinghua.edu.cn, zhao.pan@uwaterloo.ca

(Pejovic, Karney & Zhang 2004; Escaler *et al.* 2006; Torre *et al.* 2011). Particularly, the formation and collapse of cavitation bubbles can induce large pressure pulsations and heavy loads on hydraulic systems, such as pipelines and hydraulic turbines, etc. (Benjamin & Ellis 1966; Avellan 2004; Luo, Ji & Tsujimoto 2016).

An extreme case of cavitation is the formation of liquid column separation in a flow passage induced by intense transient processes. For example, when an upstream valve rapidly closes in a pipeline, the water downstream attempts to continue flowing and generates local large cavitation bubbles occupying the entire cross-section. The abrupt collapse or implosion of these large cavitation bubbles in hydraulic pipelines can cause catastrophic destruction and result in casualties and substantial economic losses (Bonin 1960; Bergant, Simpson & Tijsseling 2006; Hillgren 2011).

Previous studies have discussed the propagation and superposition of pressure oscillations induced by the collapse of the cavitation bubble and water hammer in simple pipeline systems. Experimental studies mainly focused on investigating the pressure variations in the pipelines and the validation of the relevant numerical simulations (Simpson & Wylie 1991; Bergant & Simpson 1999; Karadžić, Bulatović & Bergant 2014; Adamkowski & Lewandowski 2015). In more complex systems, such as hydraulic turbines, the internal flow and pressure fields during the guide vane closing process have been numerically studied (Zhang *et al.* 2016; Liu *et al.* 2019). Their results suggest that a moderate piece-wise guide vane closing process, i.e. a mild flow deceleration, is beneficial to reduce the risk of cavitation during the transient process. Through a water-hammer estimation, it has been recognized that the amplitude of the resulting pressure surge is closely related to the oscillation period of the cavitation bubble and its size, which in turn are decided by operating factors (e.g. the initial flow velocity (Simpson & Wylie 1991; Bergant & Simpson 1999) and pressure differences in the system (Bergant *et al.* 2006)).

Besides the physical and numerical models of hydraulic systems, the so-called 'tube-arrest' method provides an equivalent and low-cost approach to produce transient cavitation bubbles. In a tube-arrest set-up, a liquid-filled tube with an initial upward-moving velocity is arrested by a stopper, causing rapid liquid deceleration and the occurrence of cavitation bubbles at the bottom of the tube (Chesterman 1952). Based on this technique, Chen & Wang (2004) were able to produce bubbles with sizes comparable to the tube diameter, forming a full liquid column separation. It was found that the volume of the cavitation bubble could be affected by the initial velocity of the tube. However, the onset criteria of a large cavitation bubble, as well as the dependence of bubble size on operational parameters in a transient process, still remains unclear.

In the present work, we proposed a new cavitation number to predict the onset of large cavitation bubbles, and put forward a Rayleigh-type model for the dynamics of a large bubble in a cylindrical tube. The analytical results of bubble size and its oscillation period are essential for estimating the pressure surge in the transient processes. A modified experimental set-up based on the tube-arrest approach was used to systematically validate the theoretical analysis.

2. Experimental set-up

The modified tube-arrest set-up used in the present research is presented in figure 1. An acrylic tube (inner diameter $d = 16, 18, 19$ and 20 mm) filled with degassed water to heights of $l = 200$–700 mm is driven upwards by stepping on an actuator until the top of the tube hits a stopper. According to the Buckingham Π theorem of dimensional analysis and knowledge of influencing factors (such as initial velocity, acceleration and pressure difference) from references in § 1, the maximum length of the generated cavitation bubble
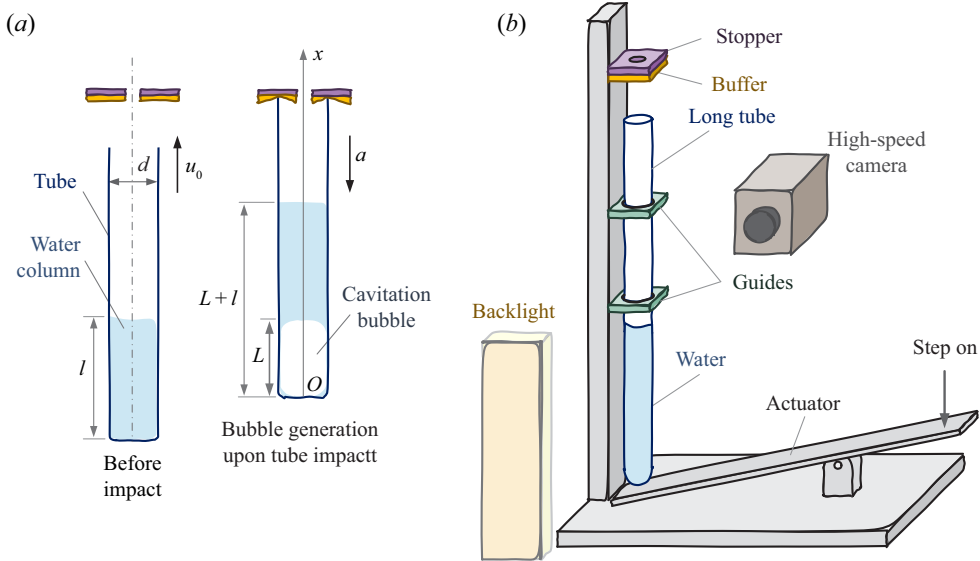
Figure 1. Experimental set-up. (*a*) Cavitation bubble generation process by tube-arrest principle and major parameters (dimensions not to scale). (*b*) Schematic of test apparatus.

can be non-dimensionalized by d and is a function of three non-dimensional groups:

$$\frac{L_{max}}{d} = F(\Pi_1, \Pi_2, \Pi_3) = F\left(\frac{\Delta p}{\rho a l}, \frac{\Delta p}{u_0^2 \rho}, \frac{l}{d}\right), \tag{2.1}$$

where u_0 and a are the tube impact velocity and acceleration upon impact, respectively, ρ is the density of the liquid, and $\Delta p = p_r - p_v$ is the pressure difference between the reference pressure p_r and the vapour pressure p_v. Thus, it is intuitive to select u_0 and a, in addition to l, as the independent variables for the experiments. In our tests, u_0 is controlled by how hard one steps on the actuator. The bottom of the stopper is attached with buffer materials (rubber and foam) with various combinations of stiffness and thickness. Taking advantage of the various cushions, a is able to be decoupled from u_0 in the tests.

The dynamics of the cavitation bubbles is recorded by a high-speed camera (Phantom V711, Vision Research, USA or FASTCAM Mini UX50, Photron, Japan) with a frame rate of 8000–10 000 f.p.s. The velocity of the tube during the process is reconstructed from the high-speed videos by tracking a marker on the tube wall, and u_0 varies from 1.0 to 6.0 m s^{-1}. The impact acceleration a (or deceleration in some engineering contexts) is measured by an accelerometer (357B03, PCB, USA) attached on the tube sampling at 102 400 Hz, and also evaluated by image processing in some cases (with a discrepancy $<10\%$ with accelerometer measurement). The acceleration for all experiments lies in the range -98 to 23 906 m s^{-2}. The bubble length L is also measured from the calibrated images directly.

The uncertainties of tube inner diameter and liquid column length are less than 1 mm and 10 mm, respectively. The impact velocity u_0 is obtained by linear regression with 10–15 measurements of the tube displacement, as the motion of the tube is nearly linear right before impact. The uncertainty corresponding to the widest 95 % confidence interval of the regression is 0.04 m s^{-1}. The nominal uncertainty of the acceleration sensor is 2 %.

Figure 2. High-speed images of typical cases of cavitation bubble(s) formed at the bottom of the tube. Here, $t = 0$ ms indicates the moment of tube impacting upon the stopper. (*a*) Small domed cavitation bubbles. (*b*) Large cylindrical cavitation bubble. (*c*) Tube burst caused by the collapse of a large cavitation bubble. Here, $d = 18$, 16, 18 mm, $l = 200$, 530, 640 mm, $u_0 = 1.91$, 3.40, 3.08 m s^{-1} and $a = 843.00$, 1857.00, 8050.00 m s^{-2}, for case (*a*), (*b*) and (*c*), respectively.

The measurement error of bubble length obtained from the image is less than 10 pixels (corresponding to ∼0.9 mm in physical dimension).

3. Onset of large cavitation bubbles

We first address the onset criteria of a cavitation bubble that is big enough to yield liquid column separation. For a cavitation bubble confined in a cylindrical tube, the size of the bubble can be characterized by its maximum length L_{max} along its axial direction.

Figure 2 shows examples of high-speed images of cavitation bubbles generated at the tube bottom. The onset of the bubble occurs immediately after the tube is arrested (at time $t = 0$ ms). In figure 2(*a*), the cavitation bubble grows (0–2.5 ms) to a domed shape and then collapses (2.5–5.1 ms). The equivalent L_{max} of the bubble is evaluated by dividing the maximum volume of the bubble by the cross-section area of the tube.

Figure 2(*b*) gives an example of a large cavitation bubble. The bubble grows to a hemisphere until its diameter approaches the inner diameter of the tube (0–3.38 ms). The bubble then undergoes growth along the tube and develops into a large cylindrical bubble to its maximum length $L_{max} = 31$ mm (at 3.38–18.38 ms). We observe that when $L_{max} > d$, water column separation is almost guaranteed to happen, and we formally address such a
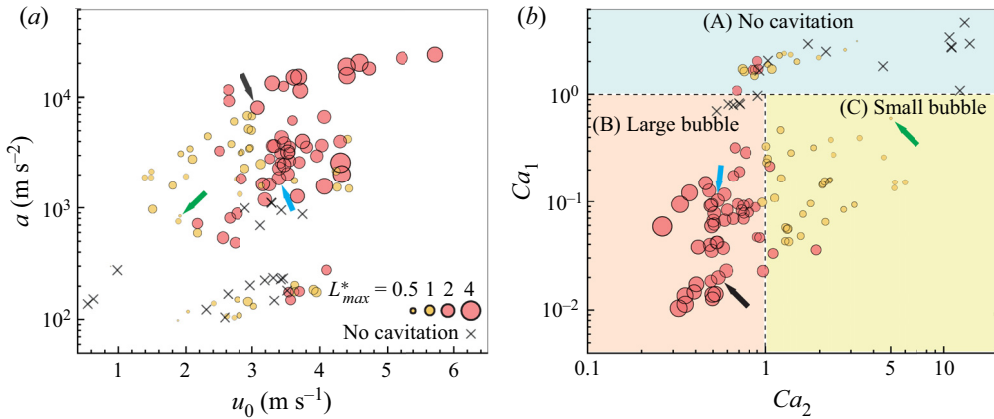
Figure 3. Dimensionless maximum bubble length L^*_{max} on (*a*) u_0 vs a and (*b*) Ca_2 vs Ca_1 phase diagrams. The areas of the filled circles indicate the values of L^*_{max} which lie in the range 0.004–4.25 in the current experiments. For $L^*_{max} \leqslant 1$ (small bubbles), the circles are filled in yellow. For $L^*_{max} > 1$, the circles are filled in red indicating large cavitation bubbles. Panel (*b*) is divided into three regimes by $Ca_1 = 1$ and $Ca_2 = 1$. Regime A ($Ca_1 > 1$) represents the no-cavitation zone. The subdomain of $Ca_1 < 1$ indicates cavitation onset, which is separated into two regimes by $Ca_2 = 1$: onset of large cavitation bubbles (regime B, $Ca_2 < 1$) and small cavitation bubbles (regime C, $Ca_2 \geqslant 1$), respectively. The particular cases illustrated in figures 2(*a*), 2(*b*) and 2(*c*) are marked with green, blue and black arrowheads, respectively.

cavity 'large cavitation bubble' hereafter. After the full water column separation, the first collapse (at 18.38–32.88 ms) happens, and subsequent decaying oscillation lasts until the bubble eventually disappears. The first bubble collapse induces the most violent pressure impulse that scales with water-hammer pressure. A rupture event of an acrylic tube was recorded in one of the preliminary tests, where a tube with a thinner wall was used, as shown in figure 2(*c*) and supplementary movie 1 available at https://doi.org/10.1017/jfm. 2021.114. This extreme case demonstrates the power of a large transient cavitation bubble.

In our set-up, the bulk motion of the water column relative to the tube upon impact can be characterized by the initial velocity and acceleration of the liquid bulk, which can be approximated by u_0 and a, respectively. The justification is as follows. Right before impact, no bubbles are formed yet and the liquid moves with the tube at u_0. Right after the tube is arrested by the stopper in a very short period of time (decelerated at a high a), the bulk water column tends to keep moving (at u_0) in the tube due to inertia, as if a piston moving in a cylinder. After that, the bulk motion of the water relative to the tube can be estimated using the length of the cavitation bubble (if any appears) by ignoring the boundary-layer effect. The boundary-layer thickness at tube sidewall δ can be estimated as $\delta = \sqrt{\nu t}$, where ν is the kinematic viscosity of the fluid and $t \sim d/u_0$ (Onuki, Oi & Tagawa 2018). Given that $u_0 \sim O(1)$ m s^{-1} and $d \sim O(10)$ mm in our experiments, $\delta/d \sim O(10^{-2})$. Thus, the influence of boundary layer on the bulk velocity and acceleration of the water column at tube impact can be neglected.

Figure 3 summarizes the experimental results of dimensionless maximum bubble length $L^*_{max} = L_{max}/d$. The results are first presented in a dimensional u_0 vs a diagram as shown in figure 3(*a*). No distinct regime of large cavitation bubbles with $L^*_{max} > 1$ distributed can be found on this diagram. Thus, the large cavitation bubble onset cannot be predicted directly using either u_0 or a. Instead, we show here that onset criteria of large cavitation bubbles can be represented with a phase diagram in terms of two non-dimensional parameters.

The first parameter is a cavitation number Ca_1 proposed by Pan *et al.* (2017):

$$Ca_1 = \frac{p_r - p_v}{\rho a l} \approx \frac{p_\infty}{\rho a l}, \tag{3.1}$$

where p_r is the reference pressure and p_v is the saturated vapour pressure of the liquid, respectively. In the current experiments, $p_\infty \approx p_r \gg p_v$ is approximately the atmosphere pressure. The static pressure of the water column, which is one order of magnitude smaller than p_∞, is neglected. This cavitation number applies to transient scenarios where the influence of liquid acceleration on pressure variation is much greater than that of the flow velocity, which is the case in our experiments. By this criterion, $Ca_1 < 1$ predicts cavitation onset.

We now investigate the size of the cavitation bubbles. Before the collision, the kinetic energy of the water column is at its maximum, which is $E_{k_{max}} = 0.5\rho\pi l(d/2)^2 u_0^2$. During the collision, the tube is arrested in a very short time while the liquid keeps the motion upwards, forming the cavitation bubble(s) at the bottom of the tube. The bubble(s) then grow (and merge) to a maximum length until the bulk velocity of the water column vanishes. Given that $p_\infty \gg p_v$, the potential energy of the bubble is approximately $E_{p_{max}} = p_\infty\pi(d/2)^2 L_{max}$ at its maximum length.

It is assumed that the energy dissipation due to pressure waves and viscosity is negligible. Balancing $E_{k_{max}}$ and $E_{p_{max}}$ gives $L_{max}/l = 0.5\rho u_0^2/p_\infty$; and further rearrangement leads to

$$Ca_2 = \frac{d}{L_{max}} = \left(\frac{d}{l}\right)\left(\frac{p_\infty}{0.5\rho u_0^2}\right) = \frac{1}{l^*}Ca_0, \tag{3.2}$$

where $l^* = l/d$ is the non-dimensional length of the water column indicating the slenderness of the water column, and $Ca_0 = p_\infty/0.5\rho u_0^2$ is the classic cavitation number. Thus, Ca_2 is a new cavitation number that can be considered as a modified version of the classic cavitation number, and Ca_2 is the second non-dimensional number to characterize the onset of the large cavitation bubble.

Rearrangement of (3.2) yields

$$L_{max}^* = Ca_2^{-1}, \tag{3.3}$$

meaning that Ca_2 (to be more specific, Ca_2^{-1}) is a direct measure of the non-dimensional maximum bubble size (i.e. the maximum cavitation length L_{max} relative to the tube diameter d). This theoretical dependence of L_{max}^* on the new cavitation number Ca_2 by (3.3) is validated, and agrees well with the experimental results, as shown in figure 4.

The onset of large cavitation bubbles requires both $Ca_1 < 1$ (onset threshold for cavitation, small or large) and $Ca_2 < 1$ (threshold for large bubbles) simultaneously. Note that $Ca_1 = \Pi_1$ and $Ca_2 = 2\Pi_2/\Pi_3$. Thus $L_{max}^* = \Pi_1^0(2\Pi_2/\Pi_3)^{-1}$. This indicates that in the context of, for example, a hydraulic system, severe water column separation occurs when (i) the valve shuts down too fast while (ii) the fluid flows too fast through a conduit that is too long. Shutting too fast corresponds to a small Ca_1: a pressure drop due to an inertial force induced by the high acceleration exceeds the tensile strength of the liquid and cavitation bubbles appear. Fluid flowing too fast through a long conduit corresponds to a small Ca_2: the kinetic energy associated with a long and fast-moving liquid column is high enough to provide the potential energy needed to generate a large bubble.

These comprehensive criteria are then validated against the experimental data on the Ca_1 vs Ca_2 diagram, as shown in figure 3(*b*). The whole domain is divided into three
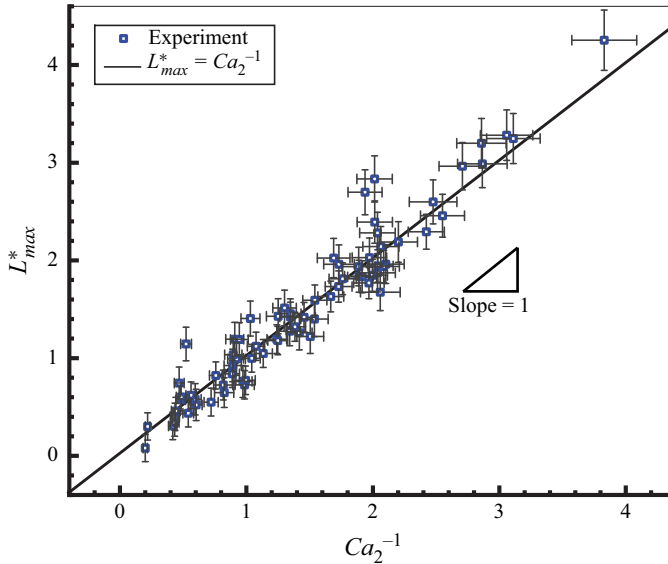
Figure 4. Experimental validation of (3.3), $L_{max}^* = Ca_2^{-1}$.

regimes by $Ca_1 = 1$ and $Ca_2 = 1$. As expected, almost all the no-cavitation events are located in regime A ($Ca_1 > 1$, blue area in figure 3); while when $Ca_1 < 1$ (red and yellow areas in figure 3, cavitation bubbles are consistently observed. These results agree with the finding in Pan *et al.* (2017). The subdomain of $Ca_1 < 1$ is further split into two regimes by $Ca_2 = 1$. Regime B ($Ca_2 < 1$, red area in figure 3) represents the criterion of large cavitation bubble onset, and regime C ($Ca_2 \geqslant 1$, yellow area in figure 3) is for small cavitation bubbles. Again, experimental data fall in the corresponding regimes and agree well with the theoretical prediction. Typical high-speed videos with no cavitation, small and large cavitation bubbles can be found in the supplementary materials.

4. Dynamics of cylindrical cavitation bubbles

We next investigate the dynamic behaviour of a large cavitation bubble. As described above (see also figure 2), a large cavitation bubble first grows radially until its interface reaches the inner wall of the tube. It then develops into a cylindrical bubble due to the confinement of the tube. Over the majority of the bubble life cycle, the cavitation bubble grows and collapses in one dimension along its axis of symmetry. This feature resembles the dynamics of bubbles in a tube with smaller scales as in Ory *et al.* (2000), Yin, Prosperetti & Kim (2004) and Sun *et al.* (2009). Based on this observation, we ignore the initial hemispherical growth of the bubble and develop a Rayleigh-type equation for the dynamics of cylindrical cavitation bubbles as follows.

As shown in figure 1, since the side boundary of the cylindrical bubble is close to the inner wall of the tube, the velocity of the liquid $u(x, t)$ can be simplified as $u(t)$. Ignoring the mass diffusion between the gas and liquid phases, the continuity equation of the liquid reads $u(t) = dL/dt$. Further ignoring the viscosity of the liquid, the Euler equation for the motion of the fluid in the x direction is

$$\rho \left(\frac{\partial u}{\partial t} + u \frac{\partial u}{\partial x} \right) = -\frac{\partial p}{\partial x}. \tag{4.1}$$
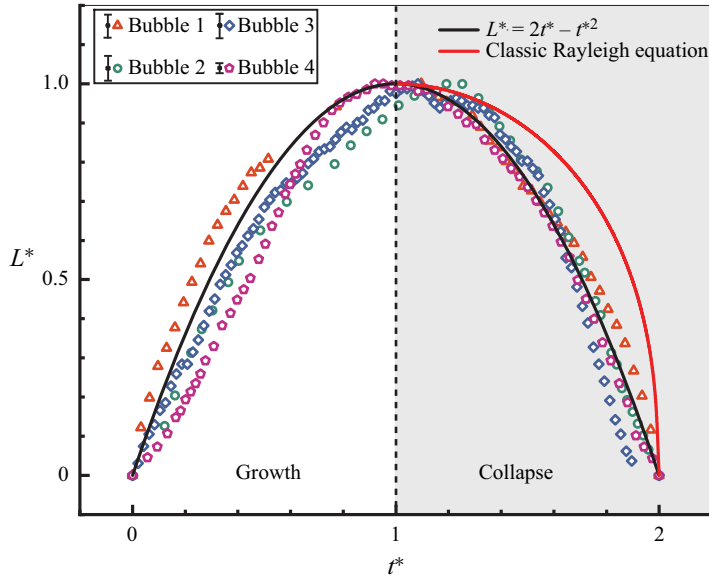
913 R6-7

Figure 5. Evolution of normalized length of cylindrical cavitation bubbles $L^* = L/L_{max}$. Here, $t^* = t/T_c$. The uncertainty of the non-dimensionalized bubble length for each case is shown next to the corresponding legend. Both experimental and theoretical results show that the growth and collapse of the bubbles are almost symmetrical over time. Compared with the infinite collapsing speed of a spherical cavitation bubble by the Rayleigh solution (red line), a cylindrical cavitation bubble has a finite collapsing velocity instead (black line).

Substituting the continuity equation into (4.1) leads to

$$\frac{\mathrm{d}^2 L}{\mathrm{d}t^2} = -\frac{1}{\rho}\frac{\partial p}{\partial x}, \qquad (4.2)$$

where $\mathrm{d}^2 L/\mathrm{d}t^2$ is the acceleration of the vapour–liquid interface. Integrating (4.2) from the top of the bubble $x = L$ to the free surface $x = L + l$, and considering pressure at the bubble boundary $p_L \approx p_v \ll p_{L+l}$, where p_{L+l} is the pressure at the free surface, the acceleration of cavitation bubble boundary can be simplified as

$$\frac{\mathrm{d}^2 L}{\mathrm{d}t^2} = -\frac{p_{L+l}}{\rho l}. \qquad (4.3)$$

Assuming the tube collides on the stopper at $t = 0$, we then have $\mathrm{d}L/\mathrm{d}t|_{t=0} = u_0$ and $L|_{t=0} = 0$ as initial conditions. Integrating (4.3) twice gives the equation for the dynamics of the cylindrical cavitation bubbles during growth and first collapse: $L = u_0 t + (1/2)(\mathrm{d}^2 L/\mathrm{d}t^2)t^2$. Further non-dimensionalization leads to

$$L^* = 2t^* - t^{*2}, \qquad (4.4)$$

where $t^* = t/T_c$, $L^* = L/L_{max}$ and T_c is the collapse time (duration from maximum length to collapse) of the bubble. The time interval between bubble onset and its first collapse is then $2T_c$. This parabolic form of bubble length over time is experimentally validated as shown in figure 5. The experimental results agree well with (4.4). Compared with the infinite collapsing speed of a spherical bubble by the Rayleigh solution, the collapse of a cylindrical bubble is 'milder' and has a finite collapse velocity u_0 instead, which is the same as the initial tube collision speed.
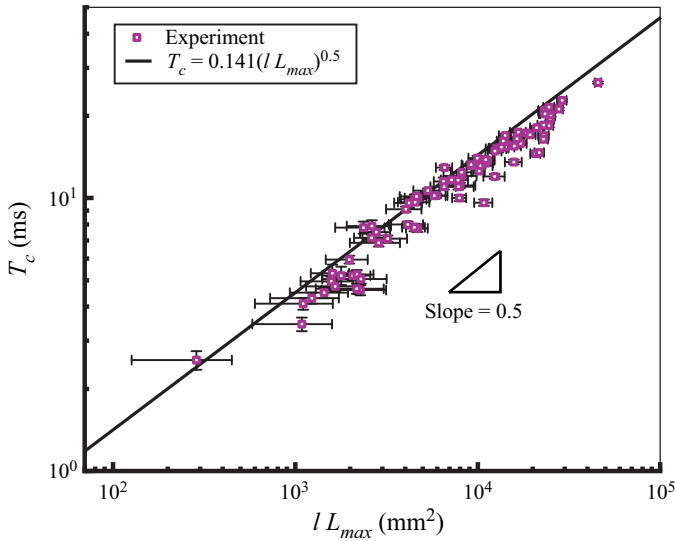
913 R6-8

Figure 6. Dependence of collapse time T_c (from maximum length to first collapse) of cylindrical cavitation bubbles on lL_{max}.

Given this knowledge, we can evaluate the water-hammer pressure in the case of figure 2(*c*) as $\rho c u_0$, where *c* is the speed of the sound in water, and $u_0 = 3.08$ m s^{-1} in the particular case. We can readily estimate the pressure impulse generated by the first collapse of the cylindrical bubble in a tube during a transient process, which is of great importance in future engineering practice, such as sudden valve closure in pipelines. Considering that $\rho \approx 1000$ kg m^{-3} and $p_\infty \approx 100\,000$ Pa for water under atmospheric pressure, the collapse time of a cylindrical cavitation bubble can be estimated as

$$T_c = \sqrt{2}\sqrt{lL_{max}}\sqrt{\frac{\rho}{p_\infty}} \approx 0.141\sqrt{lL_{max}} = 0.141\sqrt{\frac{ld}{Ca_2}}. \tag{4.5}$$

Validation of (4.5) is shown in figure 6, where T_c of cylindrical bubbles are well predicted. Note that for a spherical cavitation bubble in an infinite domain, the Rayleigh collapse time is $T_{c,R} = 0.915R_{max}\sqrt{\rho/p_\infty} \approx 0.091R_{max}$ (R_{max} is the maximum size of the spherical bubble), while for a cylindrical cavitation bubble T_c depends on both the length of the water column *l* and the maximum bubble length L_{max}. Interestingly, the length scale ($\sqrt{lL_{max}}$) in (4.5) is the geometric average of L_{max} and *l*, which is an analogy to the maximum bubble radius in the classic Rayleigh time $T_{c,R}$. It is also interesting to note that $T_c > T_{c,R}$ for bubbles with the same length scale ($\sqrt{lL_{max}} = R_{max}$), indicating a slower (and milder) collapse of a cylindrical bubble compared with a spherical one. Equation (4.5) is useful in engineering practice in order to estimate the bubble oscillation period when large cavitation bubbles are present.

5. Conclusions

In the current paper, we investigate the dynamics of a large cavitation bubble confined in a tube during a transient process by the tube-arrest technique. We focus on the onset criteria of a large bubble that can cause full water column separation, as well as the maximum length and collapse time of the cavitation bubble.

By considering energy conservation, we find that the length of the cavitation bubble in the tube can be characterized by a non-dimensional parameter $Ca_2 = l^{*-1}Ca_0$, which is a modified version of the classic cavitation number Ca_0. When $Ca_2 < 1$, large cavitation bubbles are developed in the tube. In addition, we recall the onset criteria ($Ca_1 < 1$) of cavitation bubbles during a transient process proposed by Pan *et al.* (2017). Thus, the large cavitation bubbles can only occur when both $Ca_1 < 1$ and $Ca_2 < 1$ are simultaneously satisfied. Our findings indicate that once cavitation occurs, the maximum size of cavitation bubbles is only determined by Ca_2 and is independent of Ca_1, meaning that the severity of the transient process does not affect the severity of the cavitation damage due to large bubbles. These comprehensive criteria for large cavitation bubbles are validated by systematic experiments based on the tube-arrest approach.

We also propose a Rayleigh-type equation for the dynamics of cylindrical cavitation bubbles and predicted the growth and collapse process over time. Contrary to the infinite collapse velocity of a spherical cavitation bubble as predicted by the classic Rayleigh equation, a cylindrical bubble has a finite collapse velocity equivalent to the initial impact velocity (or the speed of the liquid relative to the pipe). It is also revealed that the collapse time of the cylindrical bubble depends on not only the maximum bubble length, but also the water column length.

The results of this research may provide guidelines in the design and operation of hydraulic systems considering safety during transient processes. It should be noted that in addition to previous knowledge on transient cavitation onset, the conditions for large bubble generation, as well as the size and collapse time of large cylindrical cavitation bubbles, are mainly determined by the initial steady-state flow conditions. This finding can be applied to alleviate the damage to the hydraulic conduits from extreme cavitation that forms water column separation.

Author ORCIDs.
Zhao Pan https://orcid.org/0000-0003-1654-3205.

References

ADAMKOWSKI, A. & LEWANDOWSKI, M. 2015 Cavitation characteristics of shutoff valves in numerical modeling of transients in pipelines with column separation. *ASCE J. Hydraul. Engng* **141** (2), 04014077.
AVELLAN, F. 2004 Introduction to cavitation in hydraulic machinery. *Tech. Rep.* Politehnica University of Timişoara.
BENJAMIN, T.B. & ELLIS, A.T. 1966 The collapse of cavitation bubbles and the pressures thereby produced against solid boundaries. *Phil. Trans. R. Soc. Lond.* A **260**, 221–240.
BERGANT, A. & SIMPSON, A.R. 1999 Pipeline column separation flow regimes. *ASCE J. Hydraul. Engng* **125** (8), 835–848.
BERGANT, A., SIMPSON, A.R. & TIJSSELING, A.S. 2006 Water hammer with column separation: a historical review. *J. Fluid Struct.* **22** (2), 135–171.
BONIN, C.C. 1960 Water-hammer damage to Oigawa power station. *Trans. ASME: J. Engng Power* **82** (2), 111–116.

CHEN, Q. & WANG, L. 2004 Production of large size single transient cavitation bubbles with tube arrest method. *Chin. Phys.* **13** (4), 564–570.

CHESTERMAN, W.D. 1952 The dynamics of small transient cavities. *J. Fluid Mech.* **65** (11), 846–858.

ESCALER, X., EGUSQUIZA, E., FARHAT, M., AVELLAN, F. & COUSSIRAT, M. 2006 Detection of cavitation in hydraulic turbines. *Mech. Syst. Signal Pr.* **20** (4), 983–1007.

HILLGREN, N. 2011 *Analysis of Hydraulic Pressure Transients in the Waterways of Hydropower Stations*, 1st edn. Uppsala Universitet.

KARADŽIĆ, U., BULATOVIĆ, V. & BERGANT, A. 2014 Valve-induced water hammer and column separation in a pipeline apparatus. *Strojniški vestnik – J. Mech. Engng* **60** (11), 742–754.

LIU, K., YANG, F., YANG, Z., ZHU, Y. & CHENG, Y. 2019 Runner lifting-up during load rejection transients of a Kaplan turbine: flow mechanism and solution. *Energies* **12** (24), 4781.

LUO, X., JI, B. & TSUJIMOTO, Y. 2016 A review of cavitation in hydraulic machinery. *J. Hydrodyn.* **28** (3), 335–358.

ONUKI, H., OI, Y. & TAGAWA, Y. 2018 Microjet generator for highly viscous fluids. *Phys. Rev. Appl.* **9** (1), 014035.

ORY, E., YUAN, H., PROSPERETTI, A., POPINET, S. & ZALESKI, S. 2000 Growth and collapse of a vapor bubble in a narrow tube. *Phys. Fluids* **12** (6), 1268–1277.

PAN, Z., KIYAMA, A., TAGAWA, Y., DAILY, D.J., THOMSON, S.L., HURD, R. & TRUSCOTT, T.T. 2017 Cavitation onset caused by acceleration. *Proc. Natl Acad. Sci. USA* **114** (32), 8470–8474.

PEJOVIC, S., KARNEY, B. & ZHANG, Q. 2004 Water column separation in long tailrace tunnel. In *Hydroturbo 2004, International Conference on Hydro-Power Engineering, Brno, Czech Republic, October*, pp. 18–22.

SIMPSON, A.R. & WYLIE, E.B. 1991 Large water-hammer pressures for column separation in pipelines. *ASCE J. Hydraul. Engng* **117** (10), 1310–1316.

SUN, C., CAN, E., DIJKINK, R., LOHSE, D. & PROSPERETTI, A. 2009 Growth and collapse of a vapour bubble in a microtube: the role of thermal effects. *J. Fluid Mech.* **632**, 5–16.

TORRE, L., CERVONE, A., PASINI, A. & D'AGOSTINO, L. 2011 Experimental characterization of thermal cavitation effects on space rocket axial inducers. *Trans. ASME; J. Fluids Engng* **133** (11), 111303.

YIN, Z., PROSPERETTI, A. & KIM, J. 2004 Bubble growth on an impulsively powered microheater. *Intl J. Heat Mass Transfer* **47** (5), 1053–1067.

ZHANG, X., CHENG, Y., XIA, L. & YANG, J. 2016 CFD simulation of reverse water-hammer induced by collapse of draft-tube cavity in a model pump-turbine during runaway process. *IOP Conf.* **49** (5), 052017.